Eur. J. Mineral.
2019, **31**, 529–536
Published online 22 January 2019

Crystal chemistry of zemannite-type structures: II. Synthetic sodium zemannite

Owen P. MISSEN[1,2,a,*], Stuart J. MILLS[1] and John SPRATT[3]

[1]Geosciences, Museums Victoria GPO Box 666 Melbourne 3001 Victoria Australia
*Corresponding author, e-mail: omissen@museum.vic.gov.au
[2]School of Chemistry, University of Melbourne 3010 Victoria Australia
[3]Department of Core Research Laboratories, Natural History Museum Cromwell Road London SW7 5BD United Kingdom
[a]Now at School of Earth, Atmosphere and Environment, Monash University, Clayton 3800, Victoria, Australia.

Abstract: New zemannite-type phases, from $Na_{1.25}Fe^{3+}_{0.75}Zn_{1.25}(TeO_3)_3 \cdot 3H_2O$ to $Na_{0.55}Fe^{3+}_{1.44}Zn_{0.56}(TeO_3)_3 \cdot 3H_2O$ have been synthesised hydrothermally under basic conditions from a mixture of tellurium dioxide, zinc oxide, and either iron (III) oxide or iron (III) nitrate nonahydrate. Analysis by electron microprobe and inductively coupled plasma atomic emission spectrometry showed considerable variation in the Fe(III) and Zn contents of the framework. Single crystals of the compound produced from the iron (III) oxide syntheses were analysed, showing lower unit-cell parameters than natural zemannite, with a = 9.2620(9) and c = 7.6148(7) Å. The structure differs from type zemannite by the presence of Na and a water molecule which bridges the channel and framework by bonding *via* the oxygen atom. The unit-cell parameters of the compounds produced from iron (III) nitrate nonahydrate syntheses were refined from powder data and shown to increase with increasing pH. The results of this study show the potential for solid solution to exist in natural zemannite-type minerals and gives a stable boundary for the formation of pure zemannite-type compounds at basic pH levels, between pH 11.5 and pH 14.

Key-words: zemannite; crystal structure; tellurite; microporous; substitution; solid solution; synthesis.

1. Introduction

Several synthetic compounds, isostructural to zemannite-type minerals, have previously been prepared, including $Na_2[Zn_2(Te^{4+}O_3)_3] \cdot 2.97H_2O$ and $Na_2[Co^{2+}_2(Te^{4+}O_3)_3] \cdot 2.97H_2O$ (Miletich, 1995). Unlike the type zemannite structure, $[Mg(H_2O)_6]^{2+}$ complexes are not found in the centre of the channels in these compounds. These analogues were the first to contain Na as a confirmed channel species for a zemannite-type structure, with the Na cations found nearer the edges of the channels. Other synthetic zemannites have been synthesised; including K–Zn, K–Mn(II)–Mn(III)–Cu (Wildner, 1993) and K–Mn(II)–Cu(II) analogues (Miletich, 1995), but the structures were never published due to excessive twinning which impeded structural examination. Three selenite analogues of zemannite have also been synthesised, of which $K_2[Co^{2+}_2(SeO_3)_3] \cdot 2H_2O$ and $K_2[Ni^{2+}_2(Se^{4+}O_3)_3] \cdot 2H_2O$ have published crystal structures (Wildner, 1993). The only other published synthetic compound with a zemannite-like structure is an unusual gallium analogue, $[Ga_2(Te^{4+}O_3)_3]$-β, which consists of a neutral framework without any channel species (Kong *et al.*, 2010). The present work represents the synthetic component in the study of zemannite-type structures, which began with a study on two samples of natural zemannite (Missen *et al.*, 2019).

2. Hydrothermal synthesis

Zemannite-type phases were synthesised hydrothermally from a mixture of iron (III) nitrate nonahydrate (Sigma-Aldrich, 98%), zinc oxide (Sigma-Aldrich, 99.9%) and tellurium dioxide (Pacific Rare Metal Industries Incorporated, 99%), following a method modified from Miletich (1995). The primary reagents were mixed with 10 mL of water, adjusted to basic levels using a concentrated solution of sodium hydroxide (from pellets, Sigma-Aldrich, 98%), and reacted in a Teflon autoclave bomb in a steel sleeve at 473 K for 14 days. Reactants are summarised in Table 1. The powders produced were rinsed several times with water to remove excess nitratine ($NaNO_3$), after which they were mixed with another 10 mL of water and reacted under the same conditions for a further 7 days. Starting pH levels of 13 worked most effectively, although pure zemannite-like powders were also synthesised at pH 12 and 14. Miletich (1995) also noted that a pH of at least 9 was required for the crystallisation of synthetic zemannite-type structures.

https://doi.org/10.1127/ejm/2019/0031-2834 0935-1221/19/0031-2834 $ 3.60

Table 1. Hydrothermal synthesis materials and conditions summary (pH from aqueous NaOH).

Structure code	TeO_2 (g, mmol)	ZnO (g, mmol)	$Fe(NO_3)_3{\cdot}9H_2O$ (g, mmol)	Fe_2O_3 (g, mmol)	pH
Zemsyn	0.48, 3.0	0.12, 1.5	NA	0.8, 0.5	13
Zemsyn12	0.48, 3.0	0.12, 1.5	0.40, 1.0	NA	12
Zemsyn13	0.48, 3.0	0.12, 1.5	0.40, 1.0	NA	13
Zemsyn14	0.48, 3.0	0.12, 1.5	0.40, 1.0	NA	14

Hereon, the pure powders produced at pH 12, 13 and 14 will be referred to as zemsyn12, zemsyn13 and zemsyn14, respectively. An impure powder, mixed with unreacted oxides and zincospiroffite ($Zn_2Te^{4+}_3O_8$), was produced at pH 11 but was not analysed further in this study. No synthesis using iron (III) nitrate resulted in the production of zemannite crystals large enough for single-crystal analysis, meaning that crystallographic analysis of these zemannites was limited to determination of their unit cells.

Iron (III) oxide powder (British Drug Houses Limited, 97%) was also used in some syntheses in place of iron (III) nitrate nonahydrate to analyse any differences in the resulting products. All other conditions were kept constant, except that no post-rinsing run was required as crystals had already formed after 14 days. Zemannite was only formed from such a mixture on one occasion at pH 13; however, on this occasion the zemannite was crystalline and suitable for single-crystal analysis. Small, yellow-brown needle-like hexagonal prismatic crystals were intermingled with whitish yellow zincospiroffite, zinc tellurite ($ZnTe^{4+}O_3$) and small amounts of other unreacted powders. Hereon the synthetic zemannite crystals are referred to as zemsyn.

3. Chemistry

3.1. Electron microprobe analysis (EMPA, zemsyn crystals)

Quantitative chemical analyses of zemsyn were performed on a Cameca SX100 electron microprobe (wavelength-dispersive mode, 20 kV, 20 nA, 1 μm beam diameter and PAP matrix correction) at the Imaging and Analysis Centre, Core Research Laboratories, Natural History Museum, London. The standards used were: jadeite (for Na), corundum (Al), synthetic fayalite (Si), haematite (Fe), sphalerite (Zn) and bismuth telluride (Te). Analytical results are given in Table 2. Zemsyn yielded a composition containing essential Na, Fe, Zn and Te. Small traces of Al and Si were detected using EMPA, which were attributed to dissolution of the glass container in which the sodium hydroxide was stored. There was insufficient pure zemsyn for CHN analyses; thus H_2O was calculated based on nine framework anions (9 O) per formula unit (*pfu*), determined by the crystal-structure analysis (see below).

The empirical chemical formula is $Na_{0.83}Fe_{1.30}Al_{0.01}Zn_{0.87}Si_{0.01}Te_{2.86}H_{6.00}O_{12.00}$, which for charge balance is ideally $Na_{0.8}(Fe,Al)_{1.2}Zn_{0.8}(Te,Si)_3H_6O_{12}$. The standardised empirical formula for zemsyn is $Na_{0.8}Fe_{1.2}Zn_{0.8}(TeO_3)_3{\cdot}3H_2O$. This formula requires (in wt%) Na_2O 3.44, ZnO 9.04, Fe_2O_3 13.55, TeO_2 66.47 and H_2O 7.50, total 100 wt%.

The chemical analyses showed considerable variation of the Fe(III):Zn ratio amongst different zemsyn crystals. These data show that the zemsyn crystals analysed could be Fe or Zn dominant. Ratios varied from levels of Fe:Zn of 2.55:1, down to a few crystals in which Zn was the dominant metal (0.75:1), *i.e.* showing a wide range of solid solution compositions from $Fe_{1.44}Zn_{0.56}$ to $Fe_{0.85}Zn_{1.15}$ (Fig. 1).

3.2. ICP-AES (zemsyn12-14 powders)

A sample of each powder was weighed and digested in *aqua regia* (1 mL, 3 parts HCl to 1 part HNO_3) at 80 °C for 2 h, then diluted to 10 mL (zemsyn13) or 50 mL (zemsyn12 and zemsyn14) with deionised water and left to cool overnight.

The inductively coupled plasma atomic emission spectrometry (ICP-AES) analysis was performed on a PerkinElmer Optima 4300 DV Optical Emission Spectrometer

Table 2. Chemical analytical data for synthetic zemannite-type compounds.

	EMPA, zemsyn (21 analyses)				ICP-AES, zemsyn12		ICP-AES, zemsyn13		ICP-AES, zemsyn14	
Oxide	Average	Min	Max	St. Dev	Average	St. Dev	Average	St. Dev	Average	St. Dev
Na_2O	3.7	2.6	4.3	0.5	4.75	0.08	4.99	0.20	5.25	0.09
Al_2O_3	0.08	<dt	0.55	0.17	NA	NA	NA	NA	NA	NA
SiO_2	0.06	<dt	0.21	0.08	NA	NA	NA	NA	NA	NA
Fe_2O_3	15.1	11.6	19.6	2.0	9.43	0.12	13.59	0.27	9.44	0.35
ZnO	9.9	7.4	15.9	2.8	12.63	0.59	12.79	0.34	13.39	0.62
TeO_2	66.3	62.8	68.0	1.4	NA	NA	NA	NA	NA	NA
H_2O*	7.87	7.73	8.05	0.07						
Total	103.06				NA		NA		NA	

*Calculated based on the crystal structure (using 9 O framework anions *pfu* as a reference).

Notes. <dt indicates that a minimum value was below detection limits in EMPA, NA that the element was not analysed by ICP-AES. No totals are given for ICP-AES since Al, Si and Te were not analysed. In ICP-AES, the wavelengths of measurement (nm) were 589.592 (Na), 280.271 (Mg), 238.204 (Fe) and 206.200 (Zn).

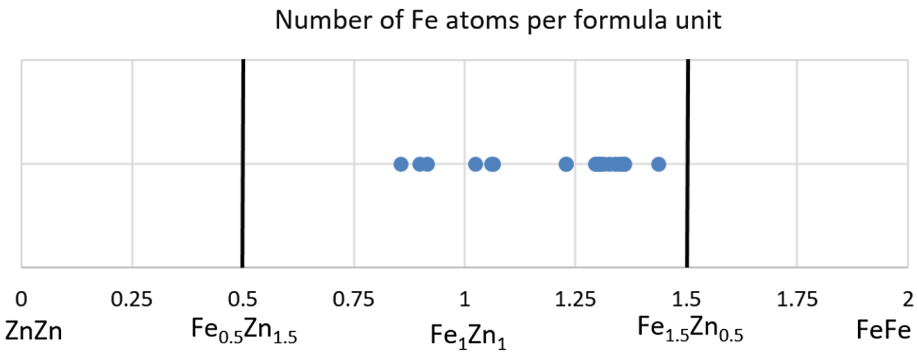

Fig. 1. Graph showing the composition variation of Fe and Zn in the zemsyn crystals by EMPA. This graph may be viewed left to right for increasing Fe and right to left for increasing Zn. The region within the vertical black lines indicate the compositional range for the mineral zemannite.

(TrACEES platform, School of Chemistry, University of Melbourne). Calibration was performed with 0.1, 1, 5, 10 and 20 mg/L solutions of Na, Mg, Mn, Fe and Zn cations with suitable soluble counter-anions. A small amount of the diluted samples was aspirated into the flame and analysed five times in quick succession, with detection at a standard wavelength of emission for each metal. The results are summarised in Table 2. The formulae of the cationic components of zemsyn12 is $Na_{1.13}Fe_{0.87}Zn_{1.14}$, zemsyn13 is $Na_{0.93}Fe_{1.05}Zn_{0.96}$, and zemsyn14 is $Na_{1.13}Fe_{0.84}Zn_{1.17}$, all based on a total charge of +6, *i.e.* all approximating an ideal formula of $Na[ZnFe^{3+}(Te^{4+}O_3)_3]\cdot 3H_2O$ if the Fe(III):Zn ratio is 1:1.

3.3. IR spectroscopic analysis

Infrared spectra were acquired from all four synthetic zemannites. Attenuated total reflection (ATR) traces were collected on a Pike Technologies GladiATR with a Bruker Tensor 27 system. The background and IR traces were determined from an average of eight scans. Scans were taken from 400 to 4000 cm^{-1}, with the transmittance recorded every 2 cm^{-1}. Results are reported in Table 3 and a representative spectrum from zemsyn12 is shown in Fig. 2.

These spectra clearly showed the broad main tellurite vibrational band centred at 656 cm^{-1}, stretching across 550–800 cm^{-1}. This peak contains both the ν_1 and ν_3 stretching vibrations. The other major vibrational band present for all zemannite samples occurred at 441 cm^{-1} and may be attributed to a water librational mode. Tellurite ν_2 and ν_4 bending modes were not visible as they occur at

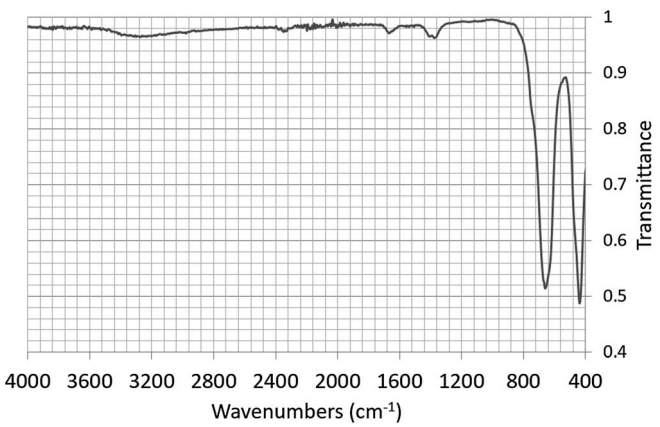

Fig. 2. A representative IR spectrum of the synthetic zemannite-type structures, zemsyn12, though all are very similar.

energies below 400 cm^{-1}. Weak, broad vibrational bands at 1668 cm^{-1} and 3235 cm^{-1} may be attributed to the H–O–H bend and the O–H stretch, respectively. The small band at 1372 cm^{-1} is attributable to the nitrate ion, present as a minor impurity from nitratine.

3.4. Chemistry discussion

The chemistry results show clear evidence of a solid solution in (synthetic) zemannite-type structures, the implications of which are further discussed below. The most interesting feature in comparing the zemannite-type structures sourced from iron (III) oxide and iron (III) nitrate is the different average Fe content. While on average the Fe:Zn content

Table 3. Tentative assignment of infrared (IR) spectroscopy peaks.

Zemannite*	zemsyn	zemsyn12	zemsyn13	zemsyn14	Average	Assignment
3300	3232	3273	3232	3201	3235	O–H
1640	1663	1670	1670	1668	1668	H–O–H
–	–	1375	1373	1369	1372	Nitrate impurity
730, 704, 690, 647	651	662	658	652	656	Tellurite ν_1 and ν_3 stretches
464, 410	453	440	438	432	441	Water librational mode

*Values taken from a naturally occurring Mn-rich zemannite (Chukanov, 2014).

in the zemsyn crystals (grown from iron (III) oxide) is $Fe_{1.2}Zn_{0.8}$ by EMPA, the Fe:Zn ratio is on average switched around in zemsyn12 and zemsyn14 ($Fe_{0.85}Zn_{1.15}$) and is close to parity in zemsyn13 at $Fe_{1.05}Zn_{0.96}$. The Na content of the channels varies with the Fe/Zn ratio, with greater Fe content typically leading to lower Na content (see Table 2). The presence of crystals from iron (III) oxide compared to polycrystalline powders from iron (III) nitrate may be explained by the different solubility of Fe (III) in these two compounds. The concentration of Fe (III) released from iron oxide would be considerably lower than from the soluble nitrate. The oxide thus is likely to promote crystal growth due to the better crystallinity of the initial crystal nuclei (Atkinson *et al.*, 1968) while the nitrate promotes seed crystal formation. The seed crystals form quickly and do not readily aggregate, leading to a polycrystalline material. Goethite nanoparticles may be synthesised in this fashion by rapid precipitation from iron (III) nitrate (Thies-Weesie *et al.*, 2007; Ou *et al.*, 2008).

4. Crystallography

4.1. Single-crystal diffraction (zemsyn)

Single-crystal X-ray diffraction of zemsyn was carried out on a SuperNova diffractometer (by Rigaku Oxford Diffraction) at the School of Chemistry, University of Melbourne, Australia. The zemsyn crystal was analysed by inserting the resin-tipped mount with the 8 × 23 × 79 μm crystal attached onto a goniometer. Data were collected at 100 K by a CCD detector and Cu $K\alpha$ radiation. The Cu radiation was used in an attempt to improve the data collection for a thin, twinned needle (following Bindi *et al.*, 2018). However, despite the use of Cu radiation, the nature of the crystal (thin needle) and the mobility of the channel species (Na cations, H_2O molecules and OH ions) result in slightly large wR_2 values. Full details of data collection and structure refinement are provided in Table 4.

A full sphere of reflection data was collected to θ = 73.010° with 99.7% completeness to θ = 67.684°. Reflection intensities were integrated, corrected for Lorentz and polarisation effects and converted to structure factors using the program CrysalisPro® (Rigaku Oxford Diffraction). Reflection merging gave an R_{int} value of 0.0476 and the full dataset was used without truncation. Although there were two strong inconsistent equivalents, testing a lower-symmetry space group (*P*6) resulted in a poorer crystal-chemical solution, meaning that the higher-symmetry space group $P6_3$ was preferred.

Structure solution was carried out by direct methods using SHELXS (Sheldrick, 2008) and structure refinement by full-matrix least-squares was implemented by SHELXL (Sheldrick, 2015) in the space group $P6_3$. An inversion-twin scale factor was refined, showing two approximately equal domains (0.52:0.48). The structure was checked for the presence of other types of twinning using *PLATON* (Spek, 2003), but no other twin laws were found. A full description of the choice of space group based on the behaviour of the framework metal octahedra for zemannite-type structures is given in Missen *et al.* (2019). *Q* peaks were found generally as crystallographic ripples around the Te atom, or in the channels as a result of the disorder of channel species. No *Q* peak was refinable in an H-atom position for the channel water molecules. The occupancy of each octahedral metal site was fixed by calculating the elemental occupancy from the average bond length of each site (Missen *et al.*, 2019). This method resulted in an *M*1 site occupancy of 81% Zn, and 19% Fe, while the *M*2 site showed complete occupancy by Fe. The occupancies of OW1 and OW2 were also refined with respect to one another, since they were too close together to occupy their respective positions simultaneously. All atom positions and anisotropic displacement parameters (U_{ij}) of framework atoms (see Table 5) were refined and converged to final R_1 and wR_2 values of 0.0507 and 0.1699, respectively. Bond lengths are summarised in Table 6 and a bond valence analysis is given in Table 7, using the parameters of Wood & Palenik (1999) for Na, Gagné & Hawthorne (2015) for Fe^{3+} and Zn, and Mills & Christy (2013) for Te^{4+}. Bond valences are reported to two decimal places due to the uncertainty associated with some bond lengths.

4.2. Crystal structure discussion (zemsyn)

Zemsyn contains narrower framework channels than natural zemannite (7.997 Å across measured O–O atom compared to 8.234 Å in type zemannite). We postulate that the elevated Fe:Zn ratio is one reason for the contraction of the channel width, as Fe(III)–O bonds are shorter than Zn–O bonds. The ratio of Fe(III):Zn was shown by bond length analysis to be 1.19:0.81, compared to type zemannite, which has a ratio of 1.04:0.96 as described by Missen *et al.* (2019). The other contributing factor to the narrower channels is the direct connection from channel to framework provided *via* Na1–OW1–Te1 linkages (see below).

Zemsyn was synthesised without any magnesium, confirming that Mg is not an essential channel species for the formation of zemannite-type structures (following Miletich, 1995). Instead hydrated sodium atoms occupy approximately four-fifths of the centre channel sites, though attempts to fix the Na occupancy for perfect charge balance were unsuccessful. The Na site is highly disordered and is located near the centre of the channels, occupying a position similar to that of Mg in natural zemannite. We attempted to move the Na off the special position, however it moved back to the same site. This is unlike previously synthesised zemannites with Na in the channels, in which the Na is found to the sides of the channels rather than in the centre (Miletich, 1995). The degree of hydration is also lowered compared to type zemannite. This occurs since less water molecules are able to fit in the smaller channels, meaning that there is less space for interstitial water as reported by Cametti *et al.* (2017).

The most interesting feature of the crystal structure of this zemannite-type compound is the positioning of the partially occupied OW1 site (Fig. 3). This oxygen atom forms a bridge between Na in the centre of the channel and Te in the framework (Na1–OW1–Te1), by means of a primary

Table 4. Crystallographic information relating to data collection and refinement of zemsyn.

Crystal data	
Ideal chemical formula	$Na_{0.5}Fe_{1.19}Zn_{0.81}(TeO_3)_3{\cdot}3H_2O$
Crystal system, space group	Hexagonal, $P6_3$
Temperature (K)	100(2)
a, c (Å)	9.2620(9), 7.6148(7)
V (Å^3)	565.72(12)
Z	2
Calculated density (g cm^{-3})	4.143
Radiation, wavelength (Å)	Cu $K\alpha$, λ = 1.54184
μ (mm^{-1})	75.023
Crystal dimensions (mm)	0.008 × 0.023 × 0.079
Crystal description	Dark orange prismatic needle
Reflections for cell refinement	323 [$I > 4\sigma(I)$]
Data collection	
Diffractometer	SuperNova (CCD detector)
θ (°) range	5.515, 73.010
Indices range of h, k, l	h: $\bar{1}0$ to 4, l: $\bar{1}0$ to 10, k: $\bar{9}$ to 8
Absorption correction	Multi-scan (SADABS, Bruker, 2001)
T_{max}, T_{min}	0.48627, 1
No. of measured, independent and observed [$I > 2\sigma(I)$] reflections	1239, 668, 541
R_{int}	0.0476
Completeness to 67.684° θ (%)	99.5
Refinement	
No. of reflections, parameters, restraints	668, 56, 1
$R_1[F^2 > 2\sigma(F^2)]$, R_1(all)	0.0518, 0.0667
$wR_2[F^2 > 2\sigma(F^2)]$, wR_2(all)	0.1756, 0.2675
GoF (F^2)	0.493
$\Delta\rho_{max}$, $\Delta\rho_{min}$ (e Å^{-3})	−1.30, 2.95 (near to octahedral metal site $M1$)

Table 5. Fractional atomic coordinates, occupancies and displacement parameters for the atomic sites of zemsyn.

Atom	x	y	z	Occ.	U_{eq}	U_{11}	U_{22}	U_{23}	U_{23}	U_{13}	U_{12}
Te1	0.45949(19)	0.49929(17)	0.1328(18)	1	0.0274(10)	0.0329(12)	0.0322(12)	0.0191(14)	−0.0010(17)	−0.001(2)	0.0178(7)
Zn1	⅔	⅓	0.3247(9)	0.8065	0.037(3)	0.049(5)	0.049(5)	0.013(5)	0	0	0.025(2)
Fe1	⅔	⅓	0.3247(9)	0.1935	0.037(3)	0.049(5)	0.049(5)	0.013(5)	0	0	0.025(2)
Fe2	⅔	⅓	−0.0533(9)	1	0.019(3)	0.021(3)	0.021(3)	0.016(7)	0	0	0.0103(15)
O1	0.666(2)	0.501(2)	0.120(6)	1	0.026(6)	0.031(9)	0.032(9)	0.017(14)	−0.013(14)	−0.022(16)	0.016(8)
O2	0.517(5)	0.663(5)	0.317(6)	1	0.028(9)	0.02(2)	0.022(15)	0.030(18)	0.014(14)	0.010(16)	0.002(13)
O3	0.511(5)	0.655(6)	−0.044(6)	1	0.036(10)	0.05(2)	0.05(2)	0.019(17)	0.015(17)	0.014(15)	0.035(17)
Na1	1	1	0.07(3)	0.5(2)	0.15(9)						
OW1	0.730(8)	0.708(9)	0.142(16)	0.31(7)	0.04(2)						
OW2	0.970(14)	1.146(14)	0.326(19)	0.69(7)	0.12(3)						

Table 6. Bond lengths (Å) comparison table for zemsyn.

Te–O2	1.85(5)	$M1$–O3 (×3)	1.97(5)
Te–O1	1.91(2)	$M1$–O1 (×3)	2.20(4)
Te–O3	1.93(5)	<$M1$–O>	2.09
Te–OW1	2.28(7)		
Te–O2	2.90(4)	Fe2–O2 (×3)	1.98(5)
Te–O3	2.93(5)	Fe2–O1 (×3)	2.04(3)
Te–O2	3.16(4)	<$M2$–O>	2.01
Te–O3	3.18(5)		
<Te–O'>	1.99	Na–OW2 (×3)	2.4(2)
<Te–O>	2.52	Na–OW2 (×3)	2.5(2)
		Na–OW1(×3)	2.66(9)
		<Na–O>	2.52

Notes. Tellurium bond length with primary bond lengths only is indicated with O'. $M1$ is the Zn dominant site and $M2$ the Fe dominant site.

bond to Te which changes the usual $Te^{4+}O_3$ trigonal pyramid formed by Te in zemannite to a $Te^{4+}O_4$ unit, which forms a distorted square pyramid (Fig. 4a). The 0.31 occupancy of OW1 adds 0.11 *vu* to each Te atom, giving a total Te bond valence of 3.93, while the total 0.13 *vu* calculated for the bridging OW1 means that it is a water molecule. The Na bond valence of 0.72 reflects its partial occupancy. The distance between O1 and OW1 is only 1.71 Å, which means that the OW1 site can only be partially occupied. The Te atoms have 8-fold coordination, with four primary and four secondary bonds forming links between three M_2O_9 dimers and one channel Na (Fig. 4b), an arrangement which is less symmetrical than the $Te^{4+}O_7$ polyhedron observed for type zemannite (Missen *et al.*, 2019), but still more symmetrical than many $Te^{4+}O_n$ polyhedra (Christy & Mills, 2013).

Table 7. Bond valence sums (in valence units, *vu*) for zemsyn*.

Atom	Te	*M*1	Fe2	Na	Σ
O1	1.13	0.26 (×3↓)	0.47 (×3↓)		1.86
O2	1.31, 0.10, 0.05		0.55 (×3↓)		2.17
O3	1.08, 0.09, 0.05	0.47 (×3↓)			1.84
OW1	0.11			0.02 (×3↓)	0.13
OW2				0.13 (×3↓), 0.10 (×3↓)	0.24
Σ	3.93	2.20	3.06	0.73	

**M*1 is the Zn dominant site. Occupancies accounted for in calculations.

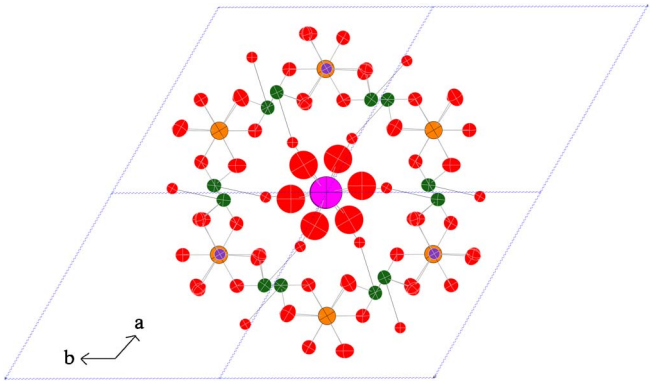

Fig. 3. A cross section of one hexagonal channel of zemsyn, viewed down *c*. Te atoms are shown in dark green, Fe atoms in purple, Zn dominant sites in orange, Na atoms in magenta and O atoms in red. Atoms are shown as thermal ellipsoids at the 70% probability level. The Te–OW1 bond is indicated with a thin line as the OW1 site is only occupied 24% of the time.

This new structure is found in a near-identical position to type zemannite in the classification system of Christy *et al.* (2016), as like all zemannite-type tellurites it contains *neso* $Te^{4+}O_3$ units which form part of a framework.

4.3. Unit-cell refinements (zemsyn12, 13 and 14 powders)

The structure of zemsyn (described above) was used as a basis for refining the unit-cell parameters of zemsyn12, zemsyn13 and zemsyn14, using the Topas program (Coelho, 2007). The powder patterns were collected on a Bruker D8 Cobalt diffractometer using Co *K*α1 radiation (λ = 1.78892 Å) from 5° to 75°, with a slit width of 0.6 mm and step size of 0.005°. The background was refined for each structure using a third-order polynomial, then the unit-cell parameters were allowed to refine, while keeping other values constant. Unit-cell and other relevant parameters are presented in Table 8. Attempts were made to determine atom occupancies and positions by full Rietveld refinement, however unrealistic Fe:Zn ratios and migration of framework oxygen atoms towards channel water sites prevented this more refined model from being used in our discussion.

The results of the unit-cell refinements show that the *a* and *c* parameters of the synthetic zemannite-type structures increase with increasing pH. Interestingly, the pH seems to have a greater influence on unit-cell parameters than does the chemical composition. When plotted against unit-cell parameter, a clear correlation is visible for pH, but no clear

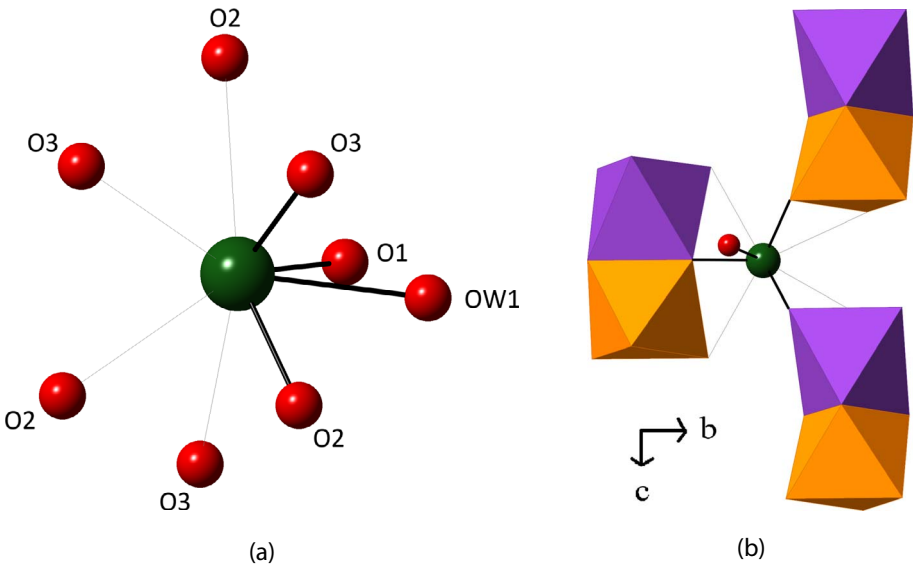

Fig. 4. Tellurium bonding in zemsyn. The three primary bonds to framework oxygen atoms and the partially occupied primary bond to OW1 are shown as thick black lines, and the four secondary bonds as grey lines. (a) Te–O bonds only. (b) Te site showing bonding with respect to the three M_2O_9 dimers it connects. OW1 is shown as a red sphere, with the Te–OW1 bond pointing towards the viewer.

Table 8. Unit-cell parameters comparison.

Sample	Diffraction type	*a*/(Å)	*c*/(Å)	Collection temperature (K)	Average composition*	Fe(III) source	Synthesis pH
Zemsyn	Single crystal	9.2620(9)	7.6148(7)	100	$Fe_{1.20}Zn_{0.80}$	Oxide	13
Zemsyn12	Powder	9.3669(7)	7.6481(6)	293	$Fe_{0.86}Zn_{1.14}$	Nitrate	12
Zemsyn13	Powder	9.3685(4)	7.6661(4)	293	$Fe_{1.04}Zn_{0.96}$	Nitrate	13
Zemsyn14	Powder	9.3948(8)	7.6746(7)	293	$Fe_{0.84}Zn_{1.16}$	Nitrate	14

*Note that composition here is normalised to two framework metal sites *pfu*.

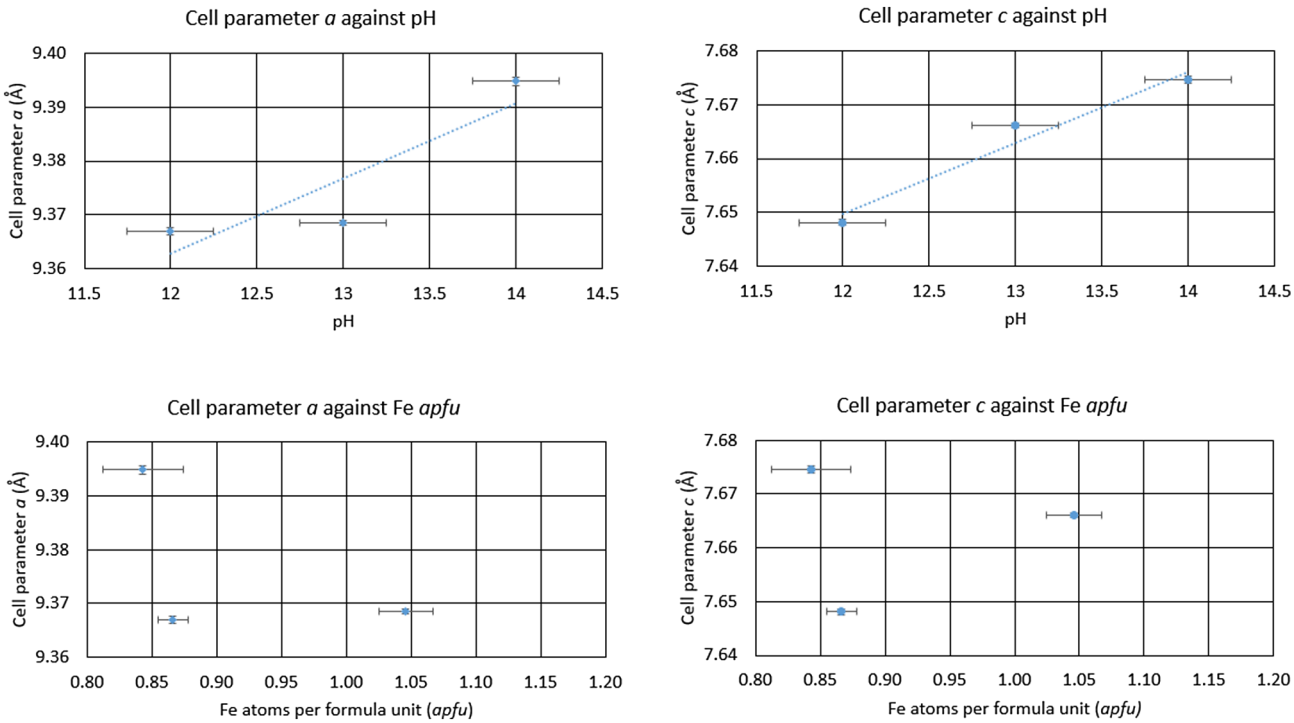

Fig. 5. Rietveld parameter graphs showing increasing parameter length with pH for the unit-cell parameters *a* and *c*, and a lack of correlation between chemical composition and the unit-cell parameters *a* and *c*.

correlation exists for the Fe:Zn ratio (see Fig. 5). These parameters are also greater than those for zemsyn (crystals), a result attributable to both the smearing of some diffraction spots (see Sect. 4.1 for a discussion on difficulties associated with the thin crystal) and also to low-temperature contraction (the powder diffraction patterns were collected at 293 K rather than at 100 K for the single-crystal data). The increase is linear for *c*, increasing at a rate of 0.013 Å per pH unit with a R^2 value of 0.96, while for *a* there is a sharp increase in *a* for zemsyn14, compared to the values for zemsyn12 and zemsyn13 (Fig. 5). The extra solution alkalinity appears to promote the broadening of the channels in the synthetic zemannite-type structures, although it should be noted that natural zemannite still has larger unit-cell parameters than any of the synthetic zemannite-type structures. As this broadening seems unrelated to the framework cation ratio, it is most likely related to the degree of hydration.

5. Conclusions

These results show significant (although not complete) solid solution in synthetic zemannite-like structures. This suggests that there is also a potential solid solution in natural zemannite-type minerals, with hypothetical new end-member minerals having ZnZn and FeFe compositions if the right conditions (Fe deficient or Zn deficient) are met, although electrostatic effects between adjacent octahedra may result in unstable end-members. Zemannite-type structures with Na in the channels may also be found in nature. Both of these factors will likely expand the number of zemannite-type minerals known. Such substitutions across two cationic sites are reasonably common, with perhaps the best known example coming from the olivenite group of minerals (Williams *et al.*, 2006; Chukanov *et al.*, 2007; Mills *et al.*, 2010). In addition, no zemannite-like selenites are known in nature, although they may in future be found as a new mineral(s), with synthetic examples known from Wildner (1993).

Acknowledgements: We thank Joël Brugger (Monash University) and Allan Pring (Flinders University) for providing the hydrothermal equipment in which all of the synthetic zemannites were synthesised. Barbara Etschmann (Monash University) and Joël provided valuable assistance with the

unit-cell refinement. We thank Timothy Hudson (University of Melbourne) for his expertise in collecting the crystal structure and for helpful comments and advice, Christopher Kingsbury (University of Melbourne) for his assistance in refining the structure, Augustine Doronila and Charles Croft (University of Melbourne) for their assistance with the ICP-AES analysis and Keith White and Brendan Abrahams (University of Melbourne) for helpful insights during the project. We also thank Editor-in-Chief Sergey Krivovichev and two anonymous reviewers for their comments, which significantly improved the manuscript. This study has been partly funded by The Ian Potter Foundation grant "tracking tellurium" to SJM, and a Museums Victoria 1854 Student Scholarship awarded to OPM, which we gratefully acknowledge. Microprobe work was funded through Natural Environment Research Council grant NE/M010848/1 "Tellurium and Selenium Cycling and Supply" to Chris J. Stanley (Natural History Museum, London). The authors acknowledge use of the facilities and the assistance of Ji Sheng Ma at the Monash X-ray Platform.

References

Atkinson, R.J., Posner, A.M., Quirk, J.P. (1968): Crystal nucleation in Fe(III) solutions and hydroxide gels. *J. Inorg. Nucl. Chem.*, **30**, 2371–2381.

Bruker (2001): SADABS and XPREP. Bruker AXS Inc., Madison, WI.

Bindi, L., Paar, W.H., Leblhuber, P. (2018): Gortdrumite, $Cu_{24}Fe_2Hg_9S_{23}$, from Leogang, Salzburg, Austria: Crystal structure and revision of the chemical formula. *Mineral. Mag.*, **82,** 853–861.

Cametti, G., Churakov, S., Armbruster, T. (2017): Reinvestigation of the zemannite structure and its dehydration behavior: a single-crystal X-ray and atomistic simulation study. *Eur. J. Mineral.*, **29**, 53–61.

Christy, A. & Mills, S. (2013): Effect of lone-pair stereoactivity on polyhedral volume and structural flexibility: application to $Te^{IV}O_6$ octahedra. *Acta Cryst. B*, **69**, 446–456.

Christy, A.G., Mills, S.J., Kampf, A.R. (2016): A review of the structural architecture of tellurium oxycompounds. *Mineral. Mag.,* **80**, 415–545.

Chukanov, N.V. (2014): Spectra of Mineral Species: Extended Library. Springer-Verlag, Dordrecht, 1716 p.

Chukanov, N.V., Pushcharovsky, D.Y., Zubkova, N.V., Pekov, I.V., Pasero, M., Merlino, S., Möckel, S., Rabadanov, M.K., Belakovskiy, D.I. (2007): Zincolivenite $CuZn(AsO_4)(OH)$: a new adamite-group mineral with ordered distribution of Cu and Zn. *Dokl. Earth Sci.*, **415**, 841–845.

Coelho, A.A. (2007): TOPAS-academic. Coelho Software, Brisbane.

Gagné, O.C. & Hawthorne, F.C. (2015): Comprehensive derivation of bond-valence parameters for ion pairs involving oxygen. *Acta Cryst. B*, **71**, 562–578.

Kong, F., Xu, X., Mao, J.G. (2010): A series of new ternary and quaternary compounds in the Li^{I}–Ga^{III}–Te^{IV}–O system. *Inorg. Chem.*, **49**, 11573–11580.

Miletich, R. (1995): The Synthetic Microporous Tellurites $Na_2[Me_2(TeO_3)_3]\cdot 3H_2O$ (*Me* = Zn, Co): Crystal Structure, De- and Rehydration, and Ion Exchange Properties. *Monatsh. Chem.*, **126**, 417–430.

Mills, S.J. & Christy, A.G. (2013): Revised values of the bond-valence parameters for Te^{IV}–O, Te^{VI}–O and Te^{IV}–Cl. *Acta Cryst. B*, **69**, 145–149.

Mills, S.J., Kampf, A.R., Poirier, G., Raudsepp, M., Steele, I.M. (2010): Auriacusite, $Fe^{3+}Cu^{2+}AsO_4O$, the first M^{3+} member of the olivenite group, from the Black Pine mine, Montana, USA. *Mineral. Petrol.,* **99**, 113–120.

Missen, O.P., Mills, S.J., Spratt, J., Birch, W.D., Brugger, J. (2019): Crystal chemistry of zemannite-type structures: I. A re-examination of zemannite from Moctezuma, Mexico. *Eur. J. Mineral.*, **31**, DOI: https://doi.org/10.1127/ejm/2019/0031-2806.

Ou, P., Xu, G., Ren, Z., Hou, X., Han, G. (2008): Hydrothermal synthesis and characterization of uniform α-FeOOH nanowires in high yield. *Mater. Lett.*, **62**, 914–917.

Sheldrick, G.M. (2008): A short history of SHELX. *Acta Cryst. A*, **64**, 112–122.

— (2015): Crystal structure refinement with SHELXL. *Acta Cryst. C*, **71**, 3–8.

Spek, A. (2003): Single-crystal structure validation with the program PLATON. *J. Appl. Cryst.*, **36**, 7–13.

Thies-Weesie, D.M.E., de Hoog, J.P., Hernandez Mendiola, M.H., Petukhov, A.V., Vroege, G.J. (2007): Synthesis of goethite as a model colloid for mineral liquid crystals. *Chem. Mater.*, **19**, 5538–5546.

Wildner, M. (1993): Zemannite-type selenites: crystal structures of $K_2[Co_2(SeO_3)_3]\cdot 2H_2O$ and $K_2[Ni_2(SeO_3)_3]\cdot 2H_2O$. *Mineral. Petrol.*, **48**, 215–225.

Williams, P.A., Leverett, P., Birch, W.D., Hibbs, D.E., Kolitsch, U., Mihajlović, T. (2006): Zinc-rich zincolibethenite from Broken Hill, New South Wales. *Aust. J. Mineral.*, **12**, 3–7.

Wood, R.M. & Palenik, G.J. (1999): Bond valence sums in coordination chemistry. Sodium–Oxygen complexes. *Inorg. Chem.*, **38**, 3926–3930.

Received 5 July 2018
Modified version received 21 November 2018
Accepted 3 December 2018